Chinese Journal of
POLYMER SCIENCE

RESEARCH ARTICLE

https://doi.org/10.1007/s10118-026-3706-6
Chinese J. Polym. Sci.

Achieving High Energy Density at 200 °C in All-organic Polyimide Dielectrics Enabled by an Ultra-low Loading Multifunctional Porphyrin Crosslinker

Nan Hai, Peng Wu, Kang-Yan Chen, Qiang-Qiang Hai, Hong-Qiang Xia, Jun Zhang*, and Jie Mao*

School of Chemistry and Chemical Engineering, Ningxia University, Yinchuan 750021, China

Electronic Supplementary Information

Abstract High-temperature polymer dielectrics are critically needed for advanced power electronics; however, their performance is often compromised by charge-transfer complexes (CTC) in aromatic polyimides. To overcome this limitation, we introduced an ultra-low loading of 5,10,15,20-tetra(4-aminophenyl) porphyrin (TAPP) as a multifunctional crosslinker into a polyimide (PI) matrix. TAPP simultaneously establishes covalent crosslinking and trap engineering, and its amino groups form a robust network with PI chains, whereas the porphyrin cycle acts as an efficient deep-level charge trap, effectively suppressing CTC formation and charge migration. The optimized PCPI films exhibited a tunable non-monotonic dielectric constant while maintaining a low loss. The PCPI-0.1 sample shows a significantly enhanced breakdown strength and achieves high discharge energy densities of 8.78, 6.09, and 4.97 J·cm^{-3} at 25, 150, 200 °C, respectively, while maintaining an efficiency above 85%. Remarkably, PCPI-0.1 delivered superior energy density compared to most high-temperature polymer dielectrics reported in the literature, coupled with excellent cycling stability and aging resistance. This work presents a strategy based on ultra-low-loading crosslinking that integrates structural modulation with deep-trap engineering, offering a viable pathway to high-performance all-organic dielectrics for extreme-condition applications.

Keywords Ultra-low loading; Covalent crosslinking; Trap engineering; Charge-transfer complexes; Energy storage; High-temperature

Citation: Hai, N.; Wu, P.; Chen, K. Y.; Hai, Q. Q.; Xia, H. Q.; Zhang, J.; Mao, J. Achieving high energy density at 200 °C in all-organic polyimide dielectrics enabled by an ultra-low loading multifunctional porphyrin crosslinker. *Chinese J. Polym. Sci.* https://doi.org/10.1007/s10118-026-3706-6

INTRODUCTION

Dielectric polymers are essential for capacitive energy storage in modern electronics and power systems owing to their high dielectric breakdown strength, flexibility, and processability.[1–3] Aromatic polyimides (PIs) are considered the top choices for high-temperature applications, because of their outstanding thermal stability and mechanical properties.[4,5] With the rapid development of cutting-edge technologies such as electric vehicles (140–150 °C), aerospace power systems (175–250 °C), and underground oil and gas exploration (170–250 °C),[6–8] the demand for PI-based dielectrics with high energy density, high charge-discharge efficiency, and reliable performance has become increasingly urgent.

However, high-performance engineering plastics, such as PI, face a major challenge: the intrinsic charge-transfer complexes (CTCs) formed between electron-donor (diamine) and electron-acceptor (dianhydride) segments within the polymer chain usually lead to increased electrical conductivity under combined thermal and electrical stress.[9,10] This leads to considerable conduction loss, severely degrading the charge-discharge efficiency and high-temperature energy density.[11] The introduction of deep-level traps is an effective strategy to suppress charge migration. The current common approaches include the incorporation of wide-bandgap nanofillers[12] or organic semiconductor molecules.[13] Inorganic fillers can induce electric field distortion from dielectric mismatch, but achieving uniform dispersion of organic or inorganic additives remains challenging, often impairing the films' mechanical integrity and processability.[12,14,15]

Recent advances in molecular-level structural design have provided a promising pathway to decouple the traditional interdependent properties of thermal stability and electrical insulation in polymer dielectrics.[13,16] In particular, the construction of crosslinked networks has proven to be effective in restricting chain mobility and introducing deep energy traps, thereby inhibiting charge migration.[17–19] Despite significant progress, conventional crosslinking strategies still face two core limitations that hinder their practical application in high-temperature energy storage dielectrics. First, most crosslinking methods require high loadings of crosslink-

* Corresponding authors, E-mail: ws1003m@163.com (J.Z.)
E-mail: maojie@nxu.edu.cn (J.M.)
Received March 12, 2026; Accepted April 7, 2026; Published online July 9, 2026

ing agents to form effective networks, which easily leads to excessive molecular packing density, intensified intermolecular interactions, and even promotion of CTC formation, resulting in a trade-off between mechanical reinforcement and electrical insulation performance.[20–22] Second, traditional crosslinkers only play a single structural crosslinking role, lacking the functional design of charge trap engineering; the constructed crosslinked networks cannot actively capture charge carriers, and the ability to suppress high-temperature charge migration is thus limited. Thus, designing a multifunctional crosslinking strategy with ultra-low loading that can simultaneously realize structural crosslinking (to suppress CTC) and trap engineering (to localize charges) has become the key to overcoming the performance bottleneck of PI high-temperature dielectrics.

Herein, we introduce a strategy employing an ultralow loading of 5,10,15,20-tetra(4-aminophenyl) porphyrin (TAPP) as a multifunctional crosslinker. As illustrated in Fig. 1, the TAPP molecule plays a dual role: its peripheral amino groups react with poly(amic acid) (PAA) chains to form a robust chemical crosslinking network, which restricts chain mobility, disrupts the inherent donor-acceptor structure of PI, and fundamentally suppresses CTC formation. The large electron-rich porphyrin macrocycle serves as an intrinsic deep-level charge trap, which can effectively localize charge carriers, increase the activation energy for charge migration, and further reduce high-temperature conduction loss. The synthesized crosslinked PCPI films exhibited distinct non-monotonic tuning of the dielectric constant while retaining an ultralow dielectric loss (tanδ<0.015). The optimized crosslinked structure PCPI-0.1 film exhibited significantly enhanced breakdown strength, measuring 741 and 475 MV·m^{-1} at 25 and 200 °C, respectively. These values correspond to a 35% and 58% increase, respectively, over those of the PI film (547 and 300 MV·m^{-1} at the respective temperatures). Moreover, the film delivers discharged energy densities (U_d), 8.78 J·cm^{-3} (η=90%) at 25 °C, 6.09 J·cm^{-3} (η=90%) at 150 °C, and 4.97 J·cm^{-3} (η=85%) at 200 °C. These values are 1.6, 1.8, and 2.1 times higher than those of the PI film (5.51 J·cm^{-3}, η=90%; 3.36 J·cm^{-3}, η=76%; 2.33 J·cm^{-3}, η=54%).This study addresses the

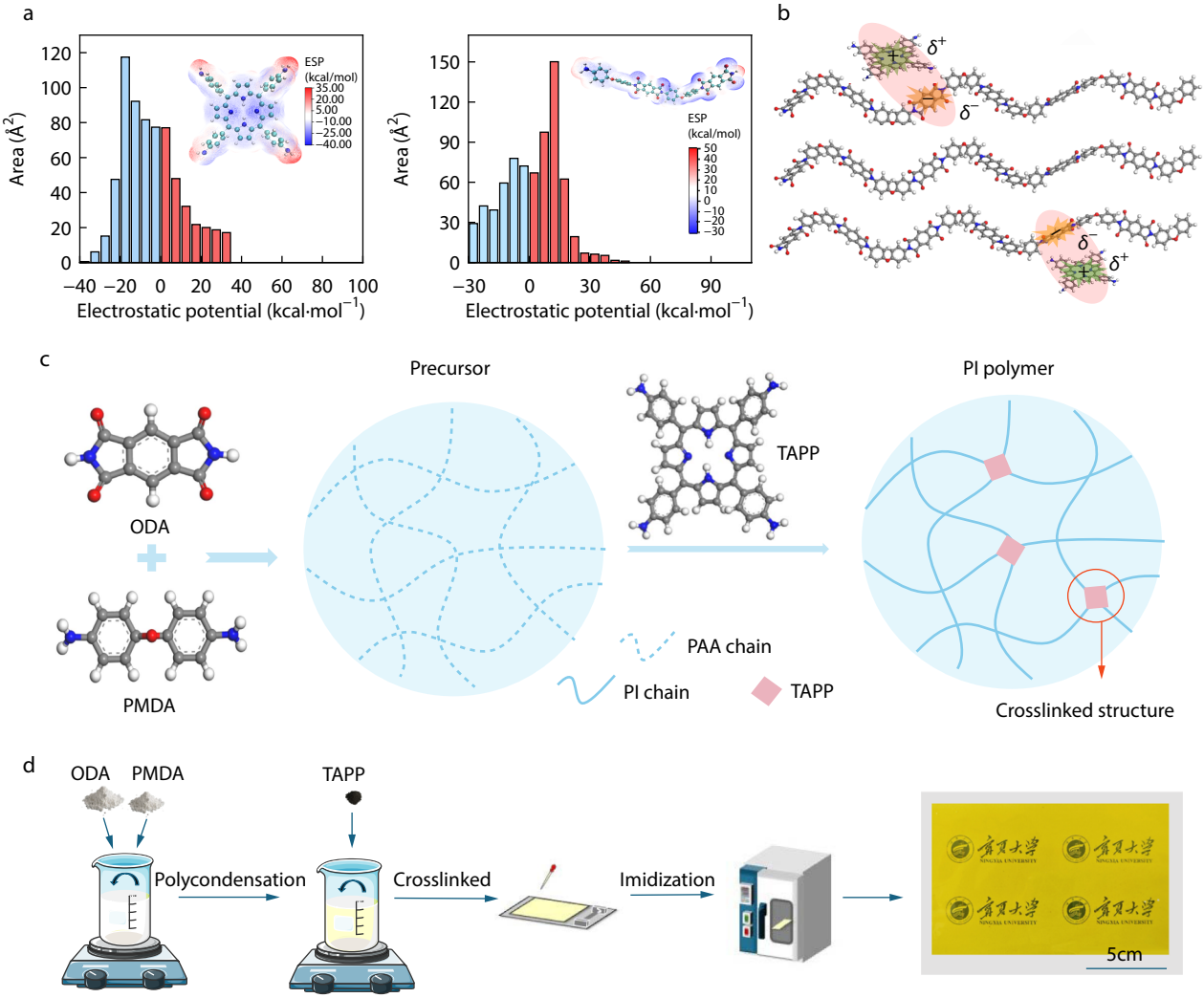

Fig. 1 (a) Electrostatic potential distribution and area percentage for TAPP and PI across different potential ranges; (b) Schematic diagram illustrating the close contact between TAPP and PI driven by electrostatic potential difference; (c) Formation of crosslinked structure; (d) Synthesis of the PCPI films.

https://doi.org/10.1007/s10118-026-3706-6

challenge of achieving high-energy-density capacitor films under extreme conditions by demonstrating a facile and effective molecular design strategy, opening a new avenue for the development of advanced all-organic dielectric materials.

EXPERIMENTAL

Materials

Pyromellitic dianhydride (PMDA) and 4,4′-oxydianiline (ODA) were obtained from Energy Chemical Co., Ltd. *N*,*N*′-dimethylformamide (DMF) was purchased from TCI Co., Ltd. The synthesis procedure of 5,10,15,20-tetrakis(4-aminophenyl) porphyrin (TAPP) is detailed in the electronic supplementary information (ESI). All the raw materials were employed without prior purification or processing.

Preparation of Polyimide (PI) films and TAPP with Crosslinked PI (PCPI) Films

The PI and PCPI films were prepared *via* a polycondensation route, as shown in Fig. 1(d) and Fig. S4 (in ESI). The synthesis commenced with ODA (8 g, 40 mmol) dissolved in DMF (60 mL) under constant nitrogen purge. Upon complete dissolution of the diamine, the reaction vessel was immersed in an ice-water bath and a stoichiometric amount of PMDA (8.812 g, 40.4 mmol) was gradually added. Stirring was continued for 24 h at low temperature to generate the PAA precursor solution. Then, varying amounts of TAPP (0.01 wt%, 0.05 wt%, 0.1 wt%, 0.5 wt%, 1 wt%, and 10 wt%, pre-dissolved in DMF (0.5 mL) were added, and the reaction proceeded for an additional 12 h to ensure complete reaction with residual anhydride termini, producing a viscous mixture. After degassing, the PAA solution was applied onto the glass substrates and spread uniformly with a 200 μm blade. The films were heated at 80 °C for 4 h, followed by a thermal imidization cycle: 100 °C (3 h), 200 °C (2 h), 250 °C (1 h), and 300 °C (1 h). The resulting translucent yellow films were subsequently detached from the blade in water and dried at 110 °C (12 h), yield the final PCPI films, which were designated based on their TAPP loading. These films are denoted as PCPI-0.01, PCPI-0.05, PCPI-0.1, PCPI-0.5, PCPI-1, and PCPI-10. Notably, the formulation with 10 wt% TAPP exhibited a pronounced tendency to gel, indicating an upper practical limit for the concentration of the crosslinking agent. For details of the experimental apparatus and test conditions, please refer to ESI.

RESULTS

Material Synthesis and Characterization

In comparison to commercial polyimide (PI), we have developed a cross-linkable PI material containing a strongly electron-deficient cyclic network core, that provides crosslinking sites and enhanced thermal stability. As illustrated in Fig. 1(a), TAPP exhibit a high electronegativity, whereas the PI matrix is positive. The substantial electrostatic potential difference strengthens intermolecular electronic interactions (Fig. 1b), leading to close contact promoted by the complementary electronic nature between TAPP's electron-rich porphyrin ring and the electron-deficient imide rings on the PI chains. Additionally, the terminal amino groups of TAPP crosslink the PAA chains via reactions with their carboxyl groups, constructing a chemical network within the PI (Fig. 1c). A pre-crosslinked polyimide was first formed at 80 °C, followed by complete crosslinking and dehydration during thermal imidization, yield the final crosslinked PI. The synthetic route is illustrated in Fig. 1(d). The resulting PCPI samples with TAPP loadings of 0.01 wt%, 0.05 wt%, 0.1 wt%, 0.5 wt%, 1 wt%, and 10 wt% are denoted as PCPI-0.01, PCPI-0.05, PCPI-0.1, PCPI-0.5, PCPI-1, and PCPI-10, respectively.

Fourier-transform infrared (FTIR) spectroscopy confirmed the successful crosslinking between TAPP and the polyimide matrix. As shown in Fig. 2(a) and Fig. S5 (in ESI), the characteristic absorption bands for both the PI and PCPI films can clearly be observed. The marked bands at 1780, 1720 and 523 cm^{-1} correspond to the bending, asymmetric stretching, and symmetric stretching vibrations of the C=O bond, respectively. Stretching vibrations of the C=N bond are responsible for the absorption feature in the range of 1600–1650 cm^{-1}. The variation in the intensity of this band across the PCPI samples corroborates the successful integration of TAPP into the PI network and the influence of the TAPP loading on the local chemical environment of the C=N bond. The band at 1360 cm^{-1} is characteristic of C—N stretching, thus verifying the formation of imide rings. The lack of any signal at 1630 or 1550 cm^{-1}, characteristic of poly(amic acid), signifies that imidization proceeded to completion in all the PI films.[23,24] The band near 1000 cm^{-1}corresponds to the in-plane C—H bending of the aromatic rings. Despite the background signal from the phenyl groups in pure PI, its intensity exhibited a systematic and significant enhancement with increasing TAPP loading, as depicted in Fig. S5 (in ESI). The emergence of a weak band at 881 cm^{-1} was due to in-plane C—H bending in the porphyrin ring, further confirming the retention of TAPP's structural integrity.

Typically, weakened long-range conjugation restricts electron delocalization in aromatic-rich polymers, resulting in a larger optical bandgap (E_g). The optical bandgap (E_g) of the PCPI films was calculated from ultraviolet-visible (UV-Vis) absorption spectra (Fig. S5 in ESI) using the Kubelka-Munk method:[25]

$$(F(R)\,hv)^{1/n} = K/S = (1-R)^2/2R = B\left(hv - E_g\right) \quad (1)$$

where the K is absorption coefficient, S is the reflection coefficient, R is the reflectivity (%), h is Planck's constant, v is the frequency of light, E_g is the energy bandgap (eV). A graph showing the relationship between $(F(R)hv)^{1/n}$ and hv was generated, and the bandgap was obtained by extrapolating the linear region to yield the value. As shown in Fig. S6 and Table S1 (in ESI), PCPI-0.1 exhibits a narrower bandgap (E_g=2.0 eV) than PI (E_g=2.39 eV). This reduction arises because the large π-conjugated system of TAPP overlaps with the localized conjugated regions in PI (such as those in the imide ring), forming an extended delocalized π-system. Consequently, the introduction of TAPP effectively narrowed the bandgap and reduced the energy required for the electron transitions.

As revealed by the Wide-angle X-ray diffraction (WAXD) patterns (Fig. 2b), all the samples exhibit only a broad and weak diffraction peak, indicative of an amorphous structure. With increasing TAPP loading, the characteristic peak shifted to lower 2θ values, from 17.45° to 17.03°. Bragg's law ($2d\sin\theta = n\lambda$)[26] was used to determine the average interchain spacing (d), where θ is the diffraction angle, and λ is the X-ray wavelength (0.15406 nm). The interchain spacing of the

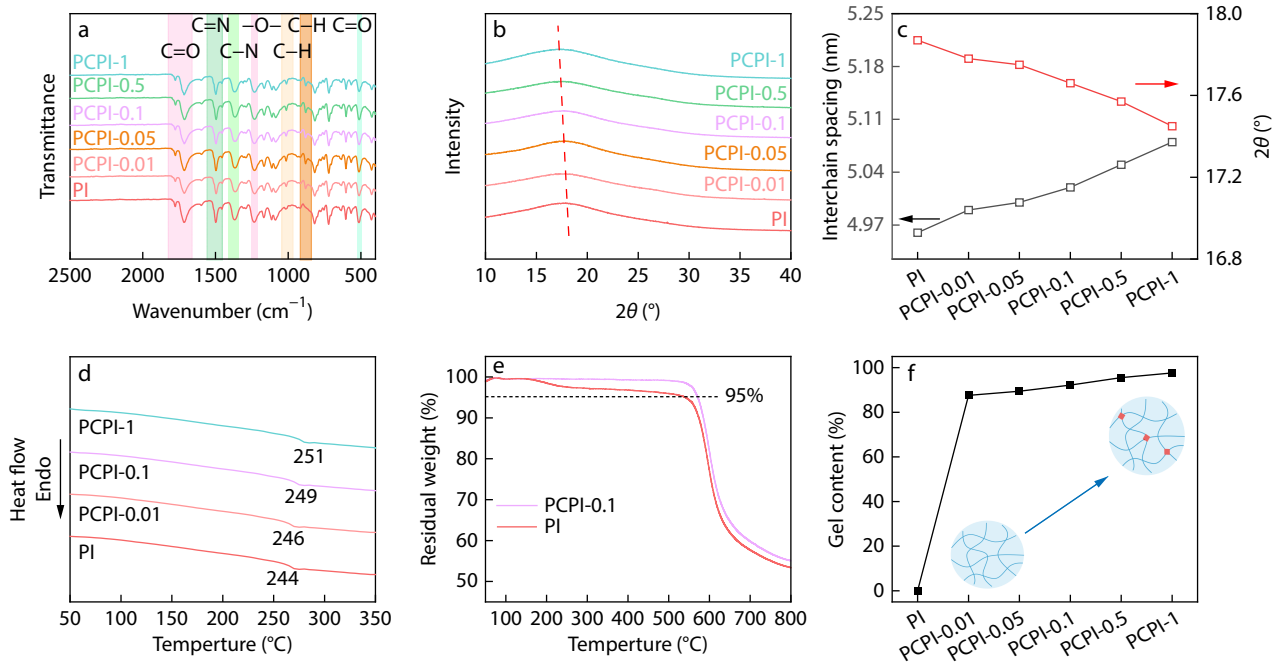

Fig. 2 Characterization of PCPI films. (a) FTIR spectra of PCPI films; (b) XRD patterns of PCPI films; (c) The interchain spacing of PCPI films; (d) DSC thermograms of PCPI films; (e) TGA thermograms of PCPI films; (f) Gel loadings of PCPI films.

PI films expands from 4.96 nm to 5.08 nm as the TAPP loading increases from 0 wt% to 1 wt% (Fig. 2c). These results suggest that the incorporation of the TAPP crosslinker disrupts the chain packing of the pristine PI, increasing the average distance between the polymer chains, thus leading to a larger *d*-spacing.

The thermal stabilities of the samples were investigated using differential scanning calorimetry (DSC) and thermogravimetric analysis (TGA). The DSC results, shown in Fig. 2(d), indicated that the glass transition temperature (T_g) increased from 244 °C for neat PI to 251 °C with increasing TAPP loading. Thermogravimetric analysis (TGA) showed that the 5% weight loss temperature ($T_{5\%}$) of PCPI-0.1 was 571 °C, significantly higher than that of PI (540 °C) (Fig. 2e). Although the increased interchain spacing might intuitively suggest a reduced packing density, the crosslinked structure restricts chain mobility and enhances thermal stability by forming a stable network that hinders thermal degradation. To further verify the crosslinked network formation, PCPI films with different TAPP loadings were immersed in DMF at 30 °C for 72 h. The insoluble fraction was washed multiple times with methanol and dried at 100 °C. As depicted in Fig. 2(f), the gel loading increased with increasing TAPP loading, from 0% for PI to 92.18% for PCPI-0.1, and 97.64% for PCPI-1, supporting the occurrence of crosslinking between the TAPP and PI chains.

The incorporation of TAPP as a crosslinking agent exhibited a pronounced concentration dependence on the mechanical properties of the PI (Fig. S7 in ESI). At low loading TAPP (0.01 wt%–0.1 wt%), the material demonstrates a synergistic improvement in both rigidity and tensile strength: Young's modulus rises from 2.44 GPa (PI) to 2.86 GPa (PCPI-0.1), while the tensile strength reaches a maximum of 166.7 MPa. These enhancements were attributed to covalent crosslinking between the imide groups of PI and the porphyrin rings of TAPP, leading to the formation of a reinforced network structure. The increase in the modulus follows the classical polymer relationship $E \propto RT/M_c$, whereby a higher crosslinking density reduces the molecular weight between crosslinks (M_c), resulting in greater stiffness. However, at higher TAPP loadings (>0.1 wt%), excessive crosslinking occurs, which reduces the elongation at break from 7.8% (PCPI-0.01) to 4.6% (PCPI-0.1) and transforms the deformation behavior from plastic to brittle. This trade-off between strength and ductility underscores the optimal balance achieved at low crosslinker loading. Importantly, marked improvements in the modulus and strength are crucial for enhancing the dielectric breakdown strength and ensuring mechanical reliability under high-field operating conditions.

Dielectric Properties and Breakdown Strength

Figs 3(a) and 3(b) present the frequency dependence of the dielectric constant (ε_r) and dielectric loss (tanδ) of the PI and PCPI films measured over the frequency range of 10^2–10^6 Hz. The ε_r value of PCPI initially decreased and then increased with increasing crosslinking degree. At 1 kHz, the lowest ε_r of PI was 3.41, while that of PCPI-0.1 was 3.08; for PCPI-1, ε_r increased to 3.74. As shown in Fig. 3(c), at low TAPP loading (≤0.1 wt%), the decrease in ε_r is primarily attributed to the porous structure of TAPP itself, followed by the effect of CTC suppression. The covalent network restricts molecular chain motion and disrupts the inherent donor-acceptor structure in PI, which suppresses charge transport but also weakens the orientational polarization of polar groups, leading to a lower dielectric constant. In this stage, the "confinement effect" of crosslinking dominates, while the polarization contribution from the TAPP porphyrin rings remains negligible. At higher TAPP loadings, the polarization behavior was dominated by induced dipole effects originating from the porphyrin units. The extensive π-conjugated

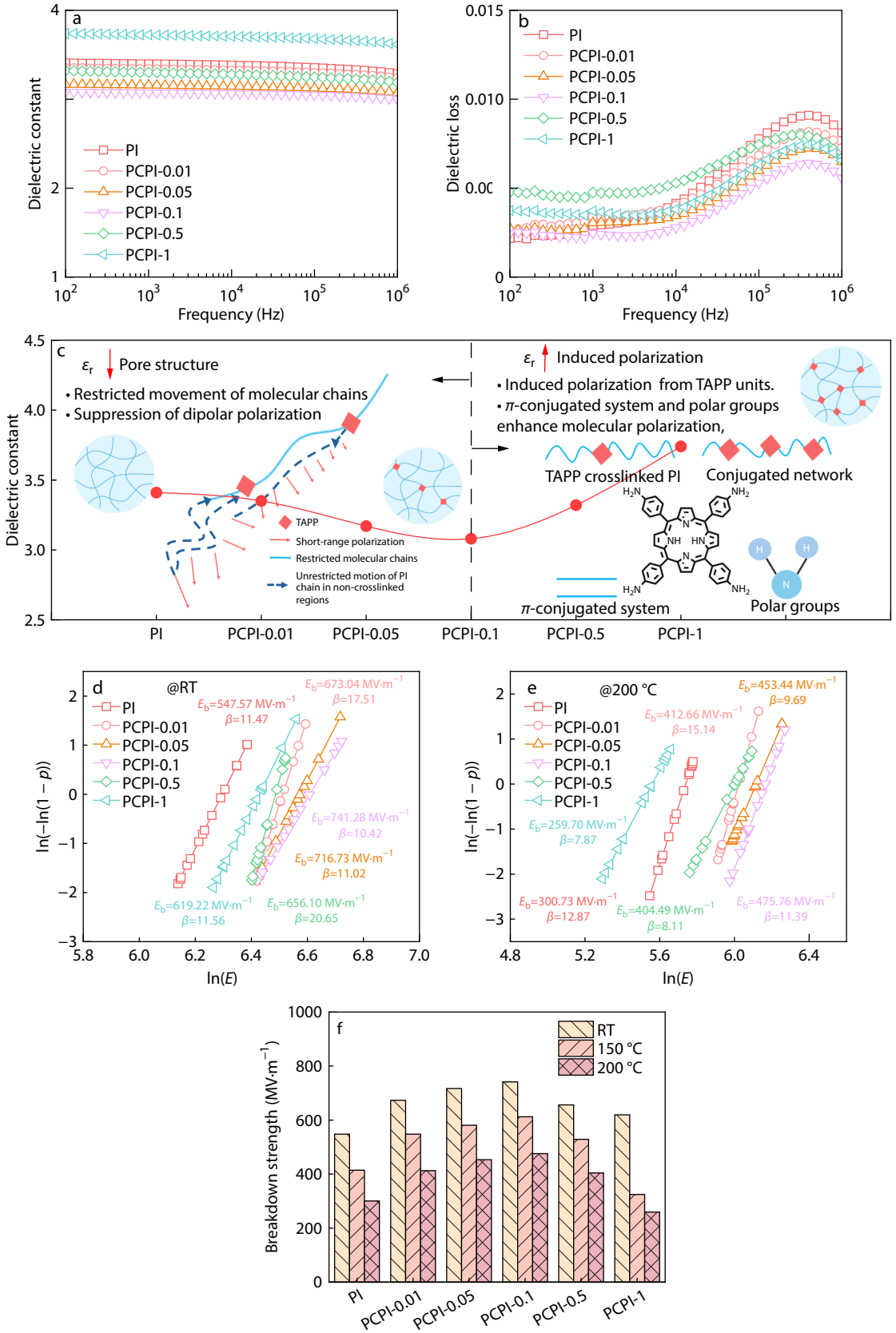

Fig. 3 (a) Frequency dependence of the dielectric constant of PI and PCPI films; (b) Frequency dependence of dielectric loss of PI and PCPI films; (c) Mechanism diagram of dielectric constant first decreasing and then increasing; Weibull breakdown distribution at (d) 25 °C and (e) 200 °C; (f) Comparative analysis of the E_b for PI and PCPI films at various temperatures.

https://doi.org/10.1007/s10118-026-3706-6

system and polar groups in TAPP significantly enhanced the intrinsic molecular polarization, compensating for the restriction caused by crosslinking. As a result, the dielectric constant recovers with increasing TAPP loading because the newly introduced polarization from the porphyrin rings outweighs the disruption of the original CTC.

All the samples maintained a low dielectric loss, with tanδ<0.015. The crosslinking action of TAPP directly suppressed CTC formation in the PI matrix, thereby reducing the generation and mobility of free charges. Simultaneously, the unique energy-level architecture of the porphyrin macrocycle serves as a deep trap, localizing charges and raising the activation energy for their migration, thereby guaranteeing an ultra-low leakage current. Specifically, PCPI-0.1 achieved the lowest dielectric loss (tanδ=0.008, at 1 kHz), which is attributed to the optimal crosslinking efficiency at this low TAPP loading. However, when the TAPP loading exceeds 0.1 wt%, molecular aggregation induced micro-defects, resulting in a moderate increase in tanδ. Despite this, the loss values for all composites remained substantially lower than that of neat PI, demonstrating the broad efficacy of the crosslinking strategy in suppressing dielectric loss.

The breakdown strengths (E_b) of the PI and PCPI films were evaluated using a two-parameter Weibull distribution. The cumulative probability of electrical failure $P(E)$ is described by:

$$P(E) = 1 - \exp\left[-(E/E_b)^{\beta}\right] \quad (2)$$

where E is the measured breakdown field, E_b is the characteristic breakdown strength at which $P(E)$ is 63.2%, and shape parameter (β) governs the reliability of the data distribution. As summarized in Figs. 3(d)–3(f) and Fig. S8 (in ESI), PCPI-0.1 exhibits a room-temperature E_b of 741 MV·m^{-1} (35% higher than PI's 547 MV·m^{-1}) and 612 MV·m^{-1} at 150 °C (48% higher than PI's 414 MV·m^{-1}), notably, at 200 °C (Fig. 3e), the value increased to 475 MV·m^{-1}, corresponding to a 58% enhancement compared to PI (310 MV·m^{-1}). The initial increase in E_b was caused by the beneficial effects of the TAPP crosslinkers. The formed interchain network suppresses CTC, whereas the porphyrin cycles act as deep-level charge traps, localize charges, and increase the activation energy for migration. This collective action mitigates space charge accumulation and leakage current, thereby delaying the thermal breakdown (Fig. 4a). Beyond the optimal concentration, excessive TAPP leads to molecular aggregation and introduces microdefects, which serve as field concentration points that promote avalanche ionization and premature breakdown. Additionally, an overly high crosslinking density can increase film brittleness and reduce tolerance to electrical stress. The more pronounced E_b improvement at 200 °C (58%) than at room temperature (35%) underscores the particular effectiveness of this strategy under high-temperature conditions, where inhibiting charge migration is crucial for preventing dielectric breakdown.

Conduction Mechanisms and Trap Effects

As the electric field intensity increased, the force exerted on the charge carriers in the material increased proportionally. When this force exceeds a certain threshold, the injected, free, or trapped charges begin to migrate directionally, generating a leakage current. To elucidate the reduction in the leakage current density, the conduction mechanism was investigated by analyzing the current density (J) versus electric field (E) characteristics. In disordered organic materials such as polyimides, charge transport is typically governed by hopping conduction between trap sites (Fig. 4b).[27] This mechanism involves the thermally activated "hopping" of trapped electrons from one localized state to another. The hopping conduction model can be described as follows:

$$J(E,T) = 2ne\lambda v \cdot \exp(-W_a/K_BT) \cdot \sinh(\lambda eE/2K_BT) \quad (3)$$

where n is the carrier concentration, λ is the jump distance, v is the thermal vibration frequency of electrons in the trap, W_a is the activation energy, e is the elementary charge, and K_B is Boltzmann's constant. Fitting of the experimental data acquired at 25 °C[28] with various conduction models (Fig. 4c) indicates that the hopping model provided the best agreement (R^2>0.98). Based on the fitting results (Fig. 4d), the jump distance for PCPI-0.1 is 0.39 nm, significantly shorter than that of pristine PI (0.81 nm), indicating enhanced charge localization. This improvement arises from two synergistic mechanisms: first, the covalent network formed by TAPP suppresses the formation of CTC between the donor and acceptor moieties in the polyimide, reducing the number of mobile charges; second, the porphyrin rings in TAPP act as deep traps, increasing the activation energy for charge de-trapping and effectively localizing carriers. Together, these effects suppress charge migration and significantly reduce the leakage current. However, at TAPP concentrations above 0.1 wt%, molecular aggregation into π-π stacks introduces interfacial defects, which act as low-resistance pathways for charge transport, thus increasing the leakage current.

The trap properties of the PI and PCPI films were evaluated using thermally stimulated depolarization current (TSDC) measurements. As shown in Fig. 4(e), the TSDC spectrum of PCPI-0.1 exhibited a higher peak temperature, stronger current intensity, and broader distribution than that of pristine PI. The trap density and energy level distribution were further quantified using an established numerical procedure implemented in MATLAB (Fig. S9 in ESI),[29] confirming that the incorporation of TAPP introduces deeper energy-level traps, which effectively immobilize charges, even at elevated temperatures.

Density functional theory (DFT) calculations were performed to elucidate the trap sites within the crosslinked and structure and determine the molecular orbital energy levels and charge distributions of PI and PCPI (Fig. 4f). TAPP exhibited a significantly lower LUMO energy level than PI, resulting in a substantial energy offset. The spatial distributions of the HOMO and LUMO (Fig. 4g and Fig. S10 in ESI) reveal a bandgap of 2.39 eV for PI, which is reduced to 2.0 eV in PCPI. Furthermore, ultraviolet photoelectron spectroscopy (UPS) (Fig. S11 in ESI) indicates that the HOMO level shifts from −5.86 eV for pristine PI to −5.32 eV upon TAPP incorporation. This trend is in good agreement with the optical band gap estimated from the $(F(R)h\nu)^2$-$h\nu$ plot (Fig. S6 in ESI). In PCPI, the LUMO is entirely localized to the TAPP unit. After charge capture by TAPP, electrons were effectively confined to the TAPP molecule, inhibiting their migration along the PI chains.

Capacitive Energy Storage Performance

The energy storage capabilities were assessed by measuring the unipolar D-E loops at room and elevated temperatures (Fig. S12 in ESI). With increasing temperature, all samples exhibited broadened D-E loops, indicating enhanced conduction loss, along with reduced breakdown strength, thus resulting in low-

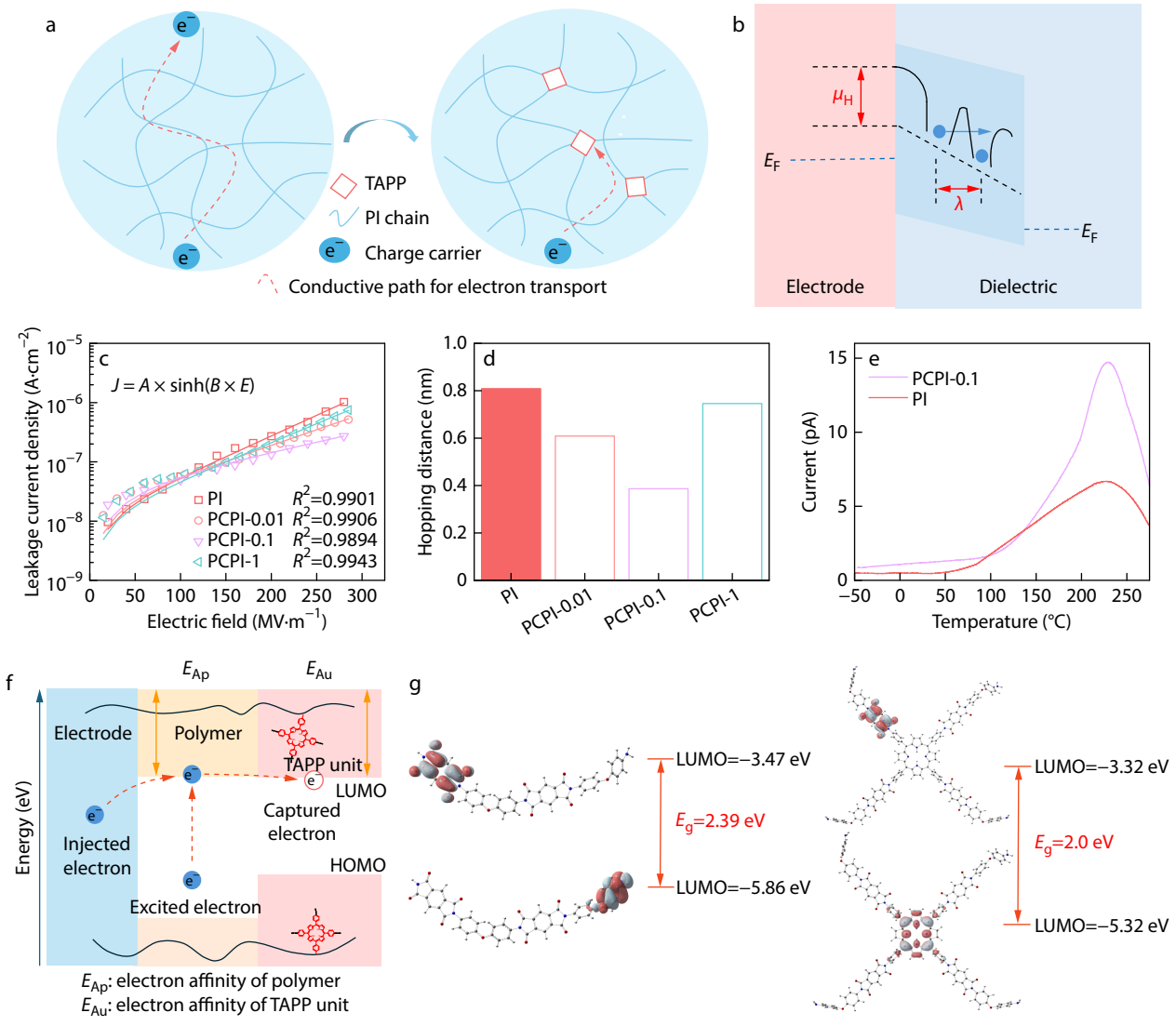

Fig. 4 (a) Breakdown mechanism diagram of PI and PCPI; (b) Schematic of the hopping conduction model (E_F: Fermi level); (c) Leakage current curves of PI and PCPI films versus electric field strength; (d) The calculated hopping distance of PI and PCPI films; (e) Thermal-stimulated depolarization current (TSDC) for PI and PCPI films; (f) The possible charge transfer mechanism in the composite visualized *via* band diagram; (g) Spatial distribution of the frontier molecular orbitals (HOMO and LUMO) in PI and PCPI.

er discharge energy density (U_d) and efficiency (η). Figs. 5(a)–5(c) and Fig. S13 (in ESI) show the U_d and η values of the PI and PCPI films at different temperatures. The PCPI-0.1 film shows a maximum U_d of 8.78 J·cm^{-3} (η=90%) at 25 °C (Fig. 5a), 6.09 J·cm^{-3} (η=90%) at 150 °C (Fig. S13 in ESI), and 4.97 J·cm^{-3} (η=85%) at 200 °C (Fig. 5b). These values are 1.6 times, 1.8 times, and 2.1 times higher than those of pristine PI (5.51 J·cm^{-3} with η=90%, 3.36 J·cm^{-3} with η=72%, and 2.33 J·cm^{-3} with η=58%), respectively. The enhanced energy storage performance originates from the multifunctional role of the TAPP crosslinker. The covalent network suppresses CTC formation, reducing mobile charge sources and polarization loss, whereas the porphyrin rings introduce deep trap levels that immobilize charges *via* high activation energy, markedly lowering conductive loss. We compared the energy storage performance of PCPI-0.1 at 200 °C with three dominant modification strategies: surface-functionalized polymers, all-organic polymers, and polymer nanocomposites. As shown in Fig. 3(d), our material delivers superior values relative to existing high-temperature dielectrics,[6,12,30–43] we selected the sample loadings from the comparative chart of energy storage performance for comparison, further confirming that the loading in our sample is ultra-low. As illustrated in Fig. 5(e), relevant data were extracted from a comparative chart of the energy storage performance for analysis. These results confirmed that the loading in our sample was ultra-low.

Reliability of Energy Storage Performance

In the industrial production of capacitor films, it is imperative that a consistent capacitive performance is maintained to ensure viable large-scale manufacturing. To verify the consistency of the energy storage performance of the continuously produced PCPI-0.1 film, six measurement points were selected on a 100 × 150 mm sample (Fig. 6a). The film was divided into 10 × 10 mm regions for thickness measurement (Fig. 6b), showing a uniform thickness ranging from 10.0 μm to 12.6 μm. Cycling sta-

bility and power density were evaluated under ambient conditions. After 10^4 charge-discharge cycles at 300 MV·m^{-1}, the U_d and η of the PCPI-0.1 film remained nearly unchanged (Fig. S13 in ESI). Under high-temperature conditions (200 °C), after 10^4 cycles in the same field, U_d and η also showed minimal variation (Fig. 6c), indicating excellent cycling stability suitable for practi-

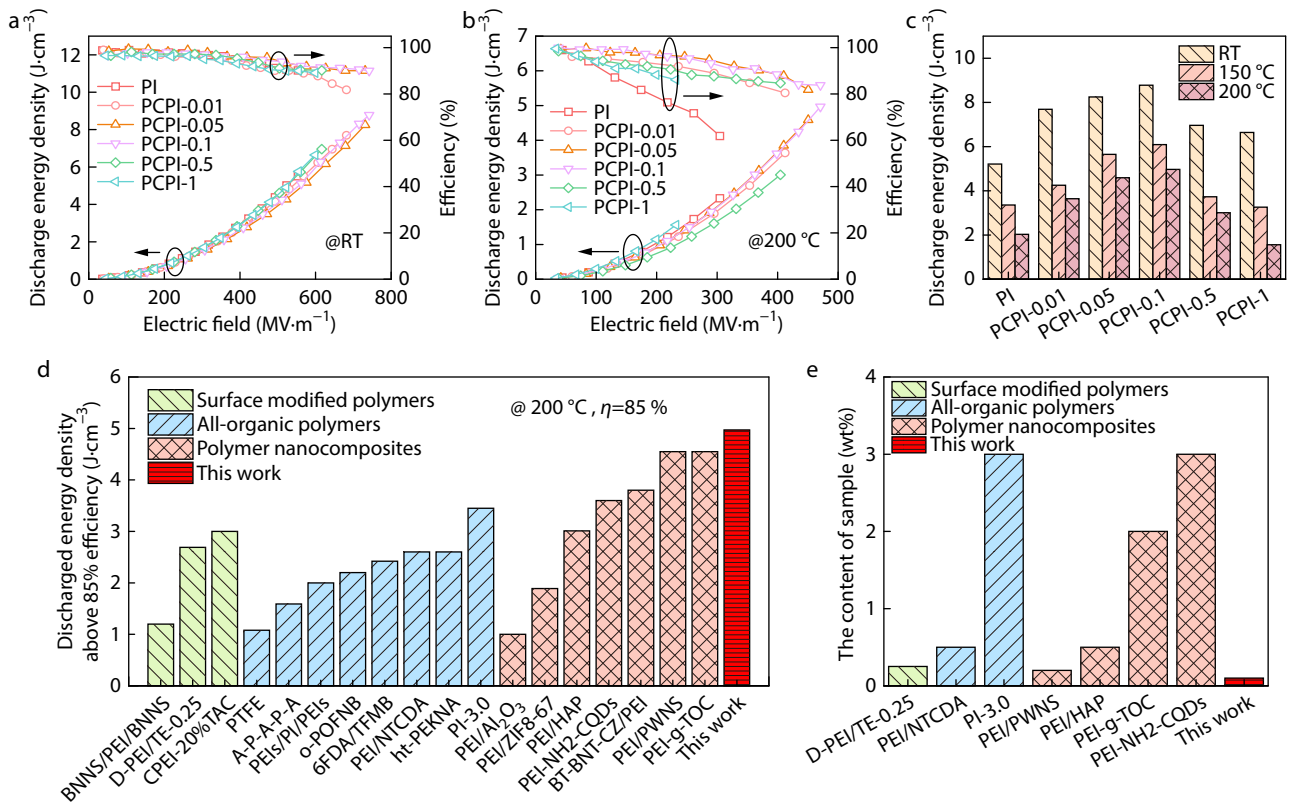

Fig. 5 (a) Energy storage performance of PI and PCPI films at 25 °C and (b) at 200 °C; (c) Comparison of energy storage performance of PI and PCPI at different temperatures; (d) Comparison of U_d at 200°C and ≥85% efficiency between the PCPI-0.1 in this work and those reported in other studies; (e) Loading of selected samples in the energy storage performance comparison chart.

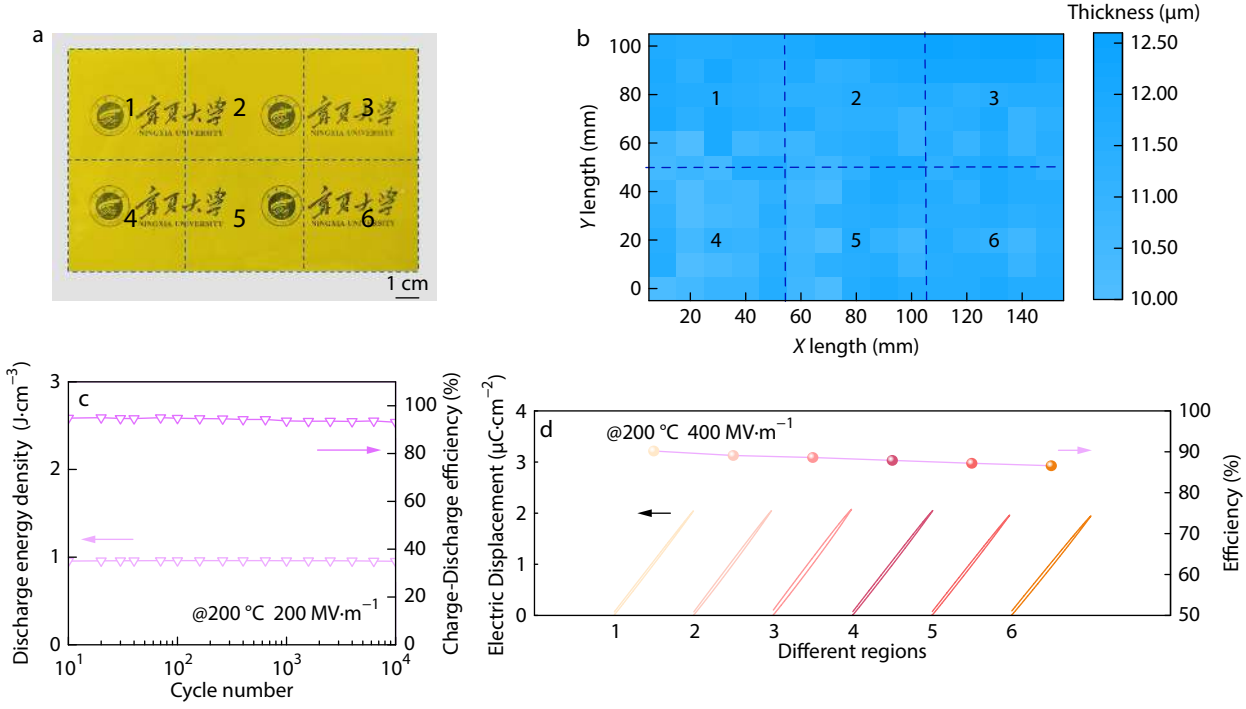

https://doi.org/10.1007/s10118-026-3706-6

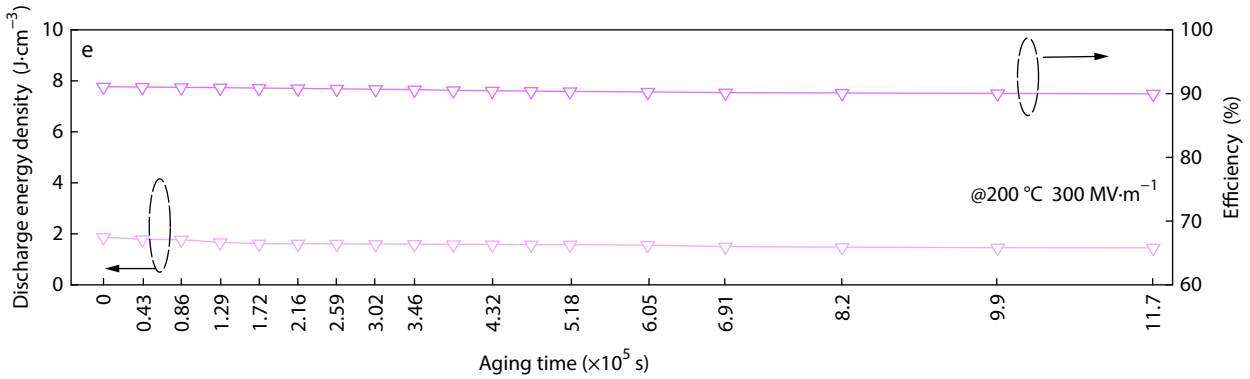

Fig. 6 (a) Test points at key locations on a capacitor film; (b) Film thickness; (c) Cyclability of PCPI-0.1 at 200 °C and 200 MV·m^{-1}: discharge energy density and efficiency over repeated charge-discharge cycles; (d) Measurement of D-E loops and charge-discharge efficiency for PCPI-0.1 at various film regions under 200 °C and 400 MV·m^{-1}; (e) The aging resistance of PCPI-0.1 at 200 °C and 300 MV·m^{-1}.

cal use. The high quality of the film under extreme conditions is evidenced by the consistent discharge energy density and charge-discharge efficiency measured at 400 MV·m^{-1} across different regions (Fig. 6d). Finally, aging tests conducted at 200 °C and 300 MV·m^{-1} validated the material's outstanding stability and aging resistance (Fig. 6e), supporting its potential for industrial production.

CONCLUSIONS

This study addresses the performance degradation of polymer dielectrics caused by charge transfer complexes (CTC) at elevated temperatures by employing ulta-lowloading TAPP as a multifunctional crosslinker to prepare PCPI films with a crosslinked architecture. A synergistic combination of structural crosslinking and trap engineering is realized through molecular design: TAPP not only establishes a covalent network with PI chains *via* its amino groups but its porphyrin cycle also functions as a deep-level trap center, effectively localizing charge carriers and suppressing charge migration. This dual-functional design integrates chemical crosslinking with molecular trapping capabilities, providing an effective strategy to inhibit CTC formation and enhance charge confinement. The optimal film (PCPI-0.1) maintained an energy efficiency above 85% across all tested temperatures, while delivering high discharged energy densities of 8.78 J·cm^{-3} at 25 °C, 6.09 J·cm^{-3} at 150 °C, and 4.97 J·cm^{-3} at 200 °C. It also showed excellent cycling stability and aging resistance under harsh conditions, demonstrating its practical relevance. The structure-function integration strategy presented here addresses key challenges in high-temperature capacitor dielectrics and provides a pathway for next-generation polymer dielectrics. Extending this approach to other cyclic systems could further improve performance and promote industrial applications in high-temperature electronics.

Conflict of Interests

The authors declare no interest conflict.

Electronic Supplementary Information

Electronic supplementary information (ESI) is available free of charge in the online version of this article at http://doi.org/10.1007/s10118-026-3706-6.

Data Availability Statement

The original raw data underlying this study have been submitted as separate supplementary files accompanying the manuscript. Additional data related to this paper may be requested from the corresponding author.

ACKNOWLEDGMENTS

This work was financially supported by the Special Project for Central Guiding Local Science and Technology Development (No. 2024FRD05061), the National Natural Science Foundation of China (No. 52503005), and Natural Science Foundation of China Ningxia Hui Autonomous Region (No. 2023AAC03016).

REFERENCES

1 Feng, Q. K.; Zhong, S. L.; Pei, J. Y.; Zhao, Y.; Zhang, D. L.; Liu, D. F.; Dang, Z. M. Recent progress and future prospects on all-organic polymer dielectrics for energy storage capacitors. *Chem. Rev.* **2022**, *122*, 3820–3878.
2 Zhang, X.; Jiang, J.; Shen, Z.; Dan, Z.; Li, M.; Lin, Y.; Shen, Y. Polymer nanocomposites with ultrahigh energy density and high discharge efficiency by modulating their nanostructures in three dimensions. *Adv. Mater.* **2018**, *30*, 1707269.
3 Li, L.; Cheng, J.; Cheng, Y.; Han, T.; Liu, Y.; Zhou, Y.; Wang, Q. Significant improvements in dielectric constant and energy density of ferroelectric polymer nanocomposites enabled by ultralow contents of nanofillers. *Adv Mater.* **2021**, *33*, 2102392.
4 Liu, X. J.; Zheng, M. S.; Chen, G.; Dang, Z. M.; Zha, J. W. High-temperature polyimide dielectric materials for energy storage: theory, design, preparation and properties. *Energ. Environ. Sci.* **2022**, *15*, 56–81.
5 Dong, J.; Li, L.; Niu, Y.; Pan, Z.; Pan, Y.; Sun, L.; Wang, H. Scalable high-permittivity polyimide copolymer with ultrahigh high-temperature capacitive performance enabled by molecular engineering. *Adv. Energy. Mater.* **2024**, *14*, 2303732.
6 H. Li, Y. Zhou, Y. Liu, L. Li, Y. Liu, Q. Wang, *CHEM SOC REV* **2021**, *50*, 6369. Li, H.; Zhou, Y.; Liu, Y.; Li, L.; Liu, Y.; Wang, Q. Dielectric polymers for high-temperature capacitive energy storage. *Chem. Soc. Rev.* **2021**, *50*, 6369–6400.
7 Zha, J. W.; Xiao, M.; Wan, B.; Wang, X.; Dang, Z. M.; Chen, G.

Graphical Abstract

Achieving High Energy Density at 200 °C in All-organic Polyimide Dielectrics Enabled by an Ultra-low Loading Multifunctional Porphyrin Crosslinker

Nan Hai, Peng Wu, Kang-Yan Chen, Qiang-Qiang Hai, Hong-Qiang Xia, Jun Zhang, and Jie Mao

Ningxia University

Ultra-low-loading 5,10,15,20-tetra(4-aminophenyl) porphyrin (TAPP) crosslinks polyimide (PI) and provides deep traps, boosting 200 °C energy density with high efficiency.

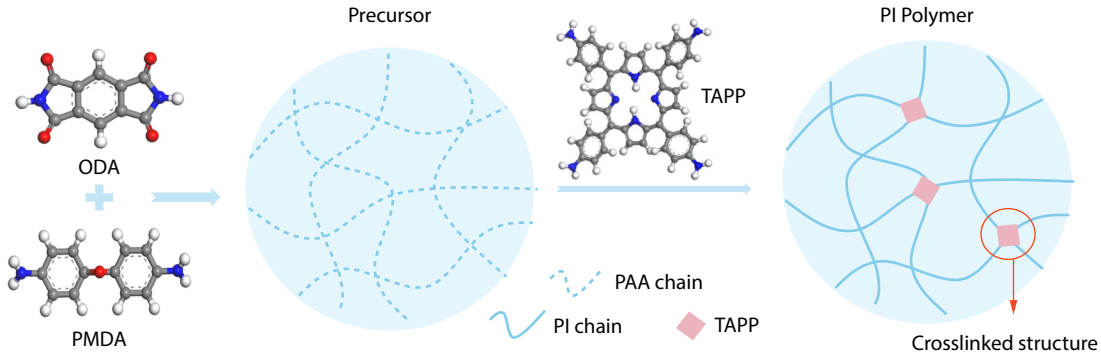

Chinese J. Polym. Sci., 2026 *https://doi.org/10.1007/s10118-026-3706-6*

Polymer dielectrics for high-temperature energy storage: constructing carrier traps. *Prog. Mater. Sci.* **2023**, *140*, 101208.

8 Hasegawa, M.; Horie, K. Photophysics, photochemistry, and optical properties of polyimides. *Prog. Polym. Sci.* **2001**, *26*, 259–335.

9 Zhuang, Y.; Seong, J. G.; Lee, Y. M. Polyimides containing aliphatic/alicyclic segments in the main chains. *Prog. Polym. Sci.* **2019**, *92*, 35–88.

10 Zhou, L.; Zhao, S.; Xie, P.; Miao, X.; Liu, S.; Sun, N.; Shen, Y. Research progress and prospect of polymer dielectrics. *Appl. Phys. Rev.* **2023**, *10*, 031310.

11 Li, L.; Dong, J.; Hu, R.; Chen, X.; Niu, Y.; Wang, H. Wide-bandgap fluorides/polyimide composites with enhanced energy storage properties at high temperatures. *Chem. Eng. J.* **2022**, *435*, 135059.

12 Yuan, C.; Zhou, Y.; Zhu, Y.; Liang, J.; Wang, S.; Peng, S.; Li, Q. Polymer/molecular semiconductor all-organic composites for high-temperature dielectric energy storage. *Nat. Commun.* **2020**, *11*, 3919.

13 Li, H.; Yang, T.; Zhou, Y.; Ai, D.; Yao, B.; Liu, Y.; Wang, Q. Enabling high-energy-density high-efficiency ferroelectric polymer nanocomposites with rationally designed nanofillers. *Adv. Funct. Mater.* **2021**, *31*, 2006739.

14 Ai, D.; Li, H.; Zhou, Y.; Ren, L.; Han, Z.; Yao, B.; Wang, Q. Tuning nanofillers in situ prepared polyimide nanocomposites for high-temperature capacitive energy storage. *Adv. Energy. Mater.* **2020**, *10*, 1903881.

15 Sun, B.; Hu, P.; Ji, X.; Fan, M.; Zhou, L.; Guo, M.; Shen, Y. Excellent stability in polyetherimide/SiO2 nanocomposites with ultrahigh energy density and discharge efficiency at high temperature. *Small* **2022**, *18*, 2202421.

16 Xiang, D.; Wang, X.; Jia, C.; Lee, T.; Guo, X. Molecular-scale electronics: from concept to function. *Chem. Rev.* **2016**, *116*, 4318–4440.

17 Wang, Q.; Wang, T.; Chi, H.; Zhao, D.; Yu, L.; Jiang, Z.; Zhang, Y. Scalable all-organic polymer dielectrics for high-temperature film capacitors with construction of deep-trap level and cross-linking network. *Chem. Eng. J.* **2025**, *506*, 160204.

18 Zhou, Y.; Zhang, Z.; Tang, Q.; Ma, X.; Hou, X. Enhancing the high-temperature energy storage properties of PEI dielectrics by constructing trap-rich covalently cross-linked networks via POSS-functionalized BNNS. *Mater. Horiz.* **2024**, *11*, 4348–4358.

19 Meng, Z.; Zhang, T.; Zhang, C.; Shang, Y.; Lei, Q.; Chi, Q. Advances in polymer dielectrics with high energy storage performance by designing electric charge trap structures. *Adv. Mater.* **2024**, *36*, 2310272.

20 Wu, C.; Deshmukh, A. A.; Li, Z.; Chen, L.; Alamri, A.; Wang, Y.; Cao, Y. Flexible temperature-invariant polymer dielectrics with large bandgap. *Adv. Mater.* **2020**, *32*, 2000499.

21 Sharma, V.; Wang, C.; Lorenzini, R. G.; Ma, R.; Zhu, Q.; Sinkovits, D. W.; Kumar, S. G Sotzing, GA; Boggs, SA; Ramprasad, R. *Nat. Commun.* **2014**, *5*, 4845.

22 Sun, Y.; Boggs, S. A.; Ramprasad, R. The intrinsic electrical breakdown strength of insulators from first principles. *Appl. Phys. Lett.* **2012**, *101*.

23 Yu, S.; Zhou, J.; Xu, A.; Lao, J.; Luo, H.; Chen, S. The scalable and high performance polyimide dielectrics containing alicyclic structures for high-temperature capacitive energy storage. *Chem. Eng. J.* **2023**, *469*, 143803.

24 Cheng, Y.; Zhang, X.; Qin, Y.; Dong, P.; Yao, W.; Matz, J.; Ye, M. Super-elasticity at 4 K of covalently crosslinked polyimide aerogels with negative Poisson's ratio. *Nat. Commun.* **2021**, *12*, 4092.

25 Landi Jr, S.; Segundo, I. R.; Freitas, E.; Vasilevskiy, M.; Carneiro, J.; Tavares, C. J. Use and misuse of the Kubelka-Munk function to

obtain the band gap energy from diffuse reflectance measurements. *Solid. State. Commun.* **2022**, *341*, 114573.
26 Pan, Y.; Guo, Y.; Liu, J.; Zhu, H.; Chen, G.; Liu, Q.; Jin, W. PDMS with tunable side group mobility and its highly permeable membrane for removal of aromatic compounds. *Angew. Chem. Int. Edit.* **2022**, *61*, e202111810.
27 Ambegaokar, V.; Halperin, B. I.; Langer, J. S. Hopping conductivity in disordered systems. *Phys. Rev. B* **1971**, *4*, 2612.
28 Chiu, F. C. A review on conduction mechanisms in dielectric films. *Adv. Mater. Sci. Eng.* **2014**, *2014*, 578168.
29 Tian, F.; Bu, W.; Shi, L.; Yang, C.; Wang, Y.; Lei, Q. Theory of modified thermally stimulated current and direct determination of trap level distribution. *J. Electrostat.* **2011**, *69*, 7–10.
30 Wu, Y.; He, Y.; Zhou, T.; Chen, C.; Zhong, F.; Xia, Y.; Zhang, C. Synergistic functionalization of h-BN by mechanical exfoliation and PEI chemical modification for enhancing the corrosion resistance of waterborne epoxy coating. *Prog. Org. Coat.* **2020**, *142*, 105541.
31 Dong, X.; Wang, Y.; Cao, Y.; Li, N.; Fu, J.; Yu, J.; Hu, Z. Enhanced high-temperature energy storage performance in all-organic dielectric films through synergistic crosslinking of chemical and physical interaction. *Chem. Eng. J.* **2024**, *500*, 157312.
32 Wei, Y.; Yang, L.; Wang, C.; Zhu, Z.; Dai, Y.; Qin, H.; Xiong, C. Enhanced high-temperature capacitive energy storage in polyetherimide dielectrics through dense crosslinked network structures. *Chem. Eng. J.* **2025**, *507*, 160793.
33 Dhanumalayan, E.; Joshi, G. M. Performance properties and applications of polytetrafluoroethylene (PTFE)-a review. *Adv. Compos. Hybrid. Ma.* **2018**, *1*, 247–268.
34 Niu, Y.; Dong, J.; He, Y.; Xu, X.; Li, S.; Wu, K.; Wang, H. Significantly enhancing the discharge efficiency of sandwich-structured polymer dielectrics at elevated temperature by building carrier blocking interface. *Nano. Energy.* **2022**, *97*, 107215.
35 Deshmukh, A. A.; Wu, C.; Yassin, O.; Mishra, A.; Chen, L.; Alamri, A.; Sotzing, G. Flexible polyolefin dielectric by strategic design of organic modules for harsh condition electrification. *Energ. Environ. Sci.* **2022**, *15*, 130–1314.
36 Qin, S.; Song, J.; Qin, H.; Fu, Y.; Liu, M.; Yu, S.; Wang, S. Fluorinated aromatic polyimide with large bandgap exhibiting superior capacitive performance at elevated temperatures. *J. Energy. Storage.* **2024**, *87*, 111458.
37 Zhou, S.; Zhao, H.; Zhang, N.; Yin, L.; Bai, J. Improved high-temperature energy storage performance of sandwich PEI-based composites via introducing charge traps by differential functional fillers. *Chem. Eng. J.* **2025**, *504*, 158941.
38 Dong, J.; Li, L.; Qiu, P.; Pan, Y.; Niu, Y.; Sun, L.; Wang, H. Scalable polyimide-organosilicate hybrid films for high-temperature capacitive energy storage. *Adv. Mater.* **2023**, *35*, 2211487.
39 Baghban, A.; Ezedin Nejadian, H.; Habibzadeh S.; Zokaee Ashtiani F.; *Sci. Rep-UK.* **2022**, *12*, 19428.
40 Choi, H.; An, J.; Lee, K.; Kwon, K. Y. Polyethyleneimine incorporated hydroxyapatite for improved colloidal stability. *Bull. Korean. Chem. Soc.* **2024**, *45*, 614–619.
41 Li, X.; Luo, H.; Zhai, D.; Wan, Y.; He, G.; Hu, D.; Zhang, S. Enhanced capacitive energy storage of polyetherimide at high temperatures by integration of electrical insulation and thermal conductivity. *Adv. Powder Mater.* **2025**, *4*, 100286.
42 Yang, M.; Li, H.; Wang, J.; Shi, W.; Zhang, Q.; Xing, H.; Shen, Y. Roll-to-roll fabricated polymer composites filled with subnanosheets exhibiting high energy density and cyclic stability at 200° C. *Nat. Energy.* **2024**, *9*, 143–153.
43 Zhao, S.; Peng, W.; Zhou, L.; Dai, S.; Ren, W.; Xu, E.; Nan, C. W. Metal-organic cage crosslinked nanocomposites with enhanced high-temperature capacitive energy storage performance. *Nat. Commun.* **2025**, *16*, 769.

https://doi.org/10.1007/s10118-026-3706-6